Analysis of gp39/CD40 Interactions Using Molecular Models and Site-Directed Mutagenesis

Jürgen Bajorath,*,‡ John S. Marken,‡,§ N. Jan Chalupny,‡,§ Tanya L. Spoon,‡ Anthony W. Siadak,‡ Marcia Gordon,‡ Randolph J. Noelle,|| Diane Hollenbaugh,‡ and Alejandro Aruffo‡

Bristol-Myers Squibb Pharmaceutical Research Institute, Seattle, Washington 98121, and Department of Microbiology, Dartmouth Medical School, Lebanon, New Hampshire 03756

Received March 2, 1995; Revised Manuscript Received May 16, 1995⊗

ABSTRACT: The interaction between gp39 (CD40L, TRAP, T-BAM) on activated T cells and mast cells and CD40 on antigen-presenting cells modulates immune responses. Gp39 and CD40 are homologous to tumor necrosis factor (TNF) and its receptor (TNFR), respectively. The TNF-β/TNFR interaction has been analyzed on the basis of mutagenesis experiments and crystal structures. Using the interaction of TNF-β/TNFR as a guide, we previously reported a site-directed mutagenesis study in which we identified residues in gp39 (K143, Y145) and CD40 (Y82, D84, N86) involved in gp39/CD40 interactions. Here we describe the use of the TNF-β/TNFR complex crystal structure as a template to prepare molecular models of gp39, CD40, and their approximate interaction. The application of these models has allowed us to extend our mutagenesis analysis of gp39/CD40 interactions. These experiments have led to the identification of additional gp39 (Y146, R203, Q220) and CD40 (E74, E117) residues that contribute to the gp39/CD40 interaction. We also further explored the importance of gp39 residue Y145 and CD40 residue Y82 for the gp39/CD40 interaction by conservatively replacing these residues with Phe. The results of these studies have enabled us to approximately outline the binding sites in gp39 and CD40. It appears that the gp39/CD40 interaction is centered on at least two clusters of residues and involves residues of two adjacent gp39 monomers. The molecular regions involved in the gp39/CD40 interaction essentially correspond to those in the homologous TNF-β/TNFR system.

The interaction between gp39 (CD40L, TRAP, T-BAM) (Armitage et al., 1992; Hollenbaugh et al., 1992; Spriggs et al., 1992; Lederman et al., 1994; Graf et al., 1992; Lane et al., 1992; Hermann et al., 1993), a type II membrane protein expressed predominantly by activated T cells and mast cells, and its receptor CD40, a type I membrane protein expressed by antigen-presenting cells (APC)[1] (Clark & Ledbetter, 1986; Paulie et al.,1985) plays a key role in the regulation of humoral immune responses. Anti-gp39 mAbs are able to block the ability of activated T cells to drive B cell proliferation and isotype switching *in vitro* (Noelle et al., 1992). The anti-murine gp39 mAb MR1 has also been shown to effectively block antibody responses to T cell-dependent antigens *in vivo* (Foy et al., 1993) as well as to prevent the onset of disease in a murine model of collagen-induced arthritis (Durie et al., 1993). Compelling evidence for the role of gp39/CD40 interactions in the regulation of antibody production comes from the analysis of defects in gp39 that lead to the absence of an effective humoral immune response in patients with X-linked hyper IgM syndrome (X-HIM) (Aruffo et al., 1993; Allen et al., 1993; Durandy et al., 1993; Korthauer et al., 1993; Di Santo et al., 1993; Fuleihan et al., 1993). Insight into the role of gp39/CD40 in the amplification of other immune functions comes from experiments which demonstrate that gp39 binding to CD40 on monocytes can regulate the expression of monocyte-derived cytokines *in vitro* (Alderson et al., 1993).

cDNA clones encoding murine (Armitage et al.,1992) and human gp39 (Graf et al.,1992; Hollenbaugh et al.,1992; Spriggs et al.,1992; Lederman et al.,1994) and human CD40 (Stamenkovic et al., 1988) revealed distinct sequence similarities (25−30%) to TNF-α and -β and TNFR, respectively (Hollenbaugh et al., 1992; Farrah & Smith, 1992; Beutler & van Huffel, 1994). Although no X-ray structures of gp39 or CD40 are currently available, crystal structures of TNF-α and -β (Eck & Sprang, 1989; Eck et al., 1992; Jones et al., 1989) and of the TNF-β/TNFR complex (Banner et al., 1993) have been reported. We have used the structures of these homologous molecules as templates to generate three-dimensional models of gp39 and CD40.

In contrast to the gp39/CD40 interaction, the molecular interactions in the TNF-β/TNFR system have been extensively characterized [for review, see Van Ostade et al. (1994)]. In a first attempt to investigate the molecular details of the gp39/CD40 interaction, we previously reported the results of a site-directed mutagenesis study in which gp39 and CD40 residues thought to participate in gp39/CD40 interactions were replaced with Ala and studied in different binding assays. The gp39 and CD40 residues targeted for replacement were selected using sequence alignments be-

* Address correspondence to this author at BMS-PRI, 3005 First Ave., Seattle, WA 98121 [telephone (206) 727-3612, Fax (206) 727-3602].

‡ Bristol-Myers Squibb Pharmaceutical Research Institute.

§ The contributions of these authors should be considered equal.

|| Dartmouth Medical School.

⊗ Abstract published in *Advance ACS Abstracts*, July 15, 1995.

[1] Abbreviations: APC, antigen-presenting cells; CD40-Ig, CD40 immunoglobulin fusion protein; FACS, fluorescence-activated cell sorter; ELISA, enzyme-linked immunosorbent assay; HRP, horseradish peroxidase; mAb, monoclonal antibody; PCR, polymerase chain reaction; rms, root mean square; sgp39, soluble recombinant gp39; TNF, tumor necrosis factor; TNFR, tumor necrosis factor receptor; X-HIM, X-linked hyper IgM syndrome.

0006-2960/95/0434-9884$09.00/0

tween gp39 and TNF-β and CD40 and TNFR and the reported crystallographic contacts (Banner et al., 1993) of the TNF-β/TNFR complex (Bajorath et al., 1995). In this analysis, gp39 residues K143 and Y145 and CD40 residues Y82, D84, and N86 were found to be critical for gp39/CD40 binding. In contrast, replacing a number of other gp39 residues (E129, S131, T135, N180, F201, E202) and CD40 residues (R73, S113, E114) with Ala had only minor or no effects on gp39/CD40 binding.

Herein we extend the analysis of residues which determine the gp39/CD40 interaction. We have prepared a TNFR-based three-dimensional model of CD40 and a TNF-β based model of gp39 using the crystal structure of the TNF-β/TNFR complex and have approximated their interactions by superposition of the models on their respective template structures. Using the models as guidance, we have targeted a number of additional gp39 and CD40 residues for site-directed mutagenesis. Furthermore, we reinvestigated the contribution of gp39 residue Y145 and CD40 residue Y82 to the gp39/CD40 interaction by carrying out more conservative replacements with Phe instead of Ala. We have identified three additional gp39 (Y146, R203, Q220) and two additional CD40 (E74, E117) residues as important for the gp39/CD40 interaction. Taken together, these studies make it possible to outline the binding sites in gp39 and CD40.

MATERIALS AND METHODS

Model Building Analysis. Computer graphics modeling and energy minimization calculations were carried out using the InsightII/Discover package (Biosym Technologies Inc., San Diego, CA). Conformational search and solvent-accessible surface (Lee & Richards, 1971) calculations were carried out using CONGEN (Bruccoleri & Novotny, 1992). For solvent-accessible surface calculations, a probe radius of 1.4 Å was used. Nonconserved loop regions and insertions and deletions in gp39 and CD40 were modeled by systematic conformational search. In each case, the conformation with minimum solvent-accessible surface within 2 kcal/mol of the energy minimum conformation was selected and included in the model. Stereochemistry, intramolecular contacts, and secondary structure of the model structures were assessed using PROCHECK (Laskowski et al., 1993). The sequence−structure compatibility of the models was assessed by energy profile analysis using the PROSAII program (Sippl, 1993). Comparative models (Bajorath et al., 1993) of the gp39 and CD40 extracellular regions were generated from structure-based sequence alignments of gp39 vs TNF-α/TNF-β and CD40 vs TNFR, respectively, using TNF-β and TNFR monomers (Banner et al., 1993) as structural templates. From the templates, all regions considered to be structurally tentative (see PDB entry pdb1tnr.ent) were deleted prior to model building. Conservative side-chain replacements were carried out in similar positions; nonconservative replacements were modeled using low-energy rotamer conformations (Bajorath & Fine, 1992). The initially built models were subjected to some minor energy minimization.

Reagents: Cell Lines, Fusion Proteins, and Antibodies. The B cell line Raji was obtained from the ATCC (Rockville, MD) and the T cell line BMS-10 from Dr. R. Mittler (Bristol-Myers Squibb, Seattle, WA). Wild-type soluble CD40-Ig, Leu8-Ig, and $_s$gp39 were previously described (Noelle et al., 1992; Hollenbaugh et al., 1992; Walz et al., 1990). The anti-murine CD8 mAb 53.6 and the anti-CD40 mAb G28-5 were a gift from Dr. J. Ledbetter (Bristol-Myers Squibb). The biotinylated anti-murine CD8 mAb Ly-2 was obtained from Caltag Laboratories (San Francisco, CA). The anti-human CD40 and gp39 mAbs 40-1.87, 40-2.210, 40-2.131, 40-1.62, 39-1.26, 39-1.59, 39-1.124, 39-1.156, 39-7.3E12 were generated and used as described (Bajorath et al., 1995).

CD40 and gp39 Mutant Proteins, Genetic Construction. Desired mutations and silent mutations for diagnostic restriction enzyme sites were introduced into cDNA fragments of the extracellular domains of either CD40 or gp39 by overlap extension PCR (Ho et al., 1989) using our previous protocol (Bajorath et al., 1995). The CD40-Ig fusion genes were prepared by subcloning the PCR-amplified CD40 extracellular domain mutants into the mammalian expression vector CDM7B$^-$ which contained a cDNA fragment encoding the hinge, CH2, and CH3 domains of human IgG1 (Noelle et al., 1992). The fusion genes encoding the mutant $_s$gp39 proteins were prepared by subcloning the PCR-amplified gp39 extracellular domain mutants into the same mammalian expression vector containing a cDNA fragment encoding the extracellular domain of murine CD8 (Lyt2a) (Hollenbaugh et al., 1992). The DNA encoding each of the mutant $_s$gp39 and CD40-Ig proteins was verified by sequencing.

Wild-Type and Mutant CD40 and gp39 Proteins, Production and Binding Assays. Wild-type and mutant CD40 and $_s$gp39 proteins were produced from transiently transfected COS cells as described (Hollenbaugh et al., 1992; Noelle et al., 1992). For SDS−PAGE analysis, COS cells were metabolically labeled with [^{35}S]methionine and cysteine (Tran^{35}S-Label, ICN, Costa Mesa, CA). The CD40-Ig fusion proteins were recovered by immunoprecipitation with immobilized protein A (Repligen Corp., Cambridge, MA). BMS-10 cells, a Jurkat cell line variant which expresses surface gp39, were incubated with wild-type or mutant CD40-Ig or a control fusion protein, Leu8-Ig (25 μg/mL, 1 h, 4 °C), followed by FITC-conjugated goat anti-human IgG Fc (1:500 dilution, 30 min, 4 °C, TAGO, Burlingame, CA). Fusion protein binding to 5×10^5 cells was analyzed by flow cytometry (FACscan, Becton Dickinson, Mountain View, CA). The binding of wild-type and mutant $_s$gp39 to CD40 expressed on the surface of the B cell line Raji was examined by flow cytometry, and the binding of wild-type and mutant CD40-Ig to immobilized $_s$gp39 was determined as described (Hollenbaugh et al., 1992). Since methods for purifying active $_s$gp39 are currently not established, assessment of binding of immobilized wild-type and mutant $_s$gp39 to CD40-Ig required that either neat or concentrated COS cell supernatants containing the different $_s$gp39 proteins be used for these studies. The presence of saturating and equal amounts of immobilized $_s$gp39 was confirmed by ELISA using a second anti-CD8 mAb (Ly-2) whose binding to the fusion protein is not affected by the presence of the 53.6 mAb (Bajorath et al., 1995).

RESULTS AND DISCUSSION

Molecular Models of gp39 and CD40. Figure 1 shows the structure-oriented sequence alignments of CD40 and TNFR (a) and gp39 and TNF-β (b) on which the modeling

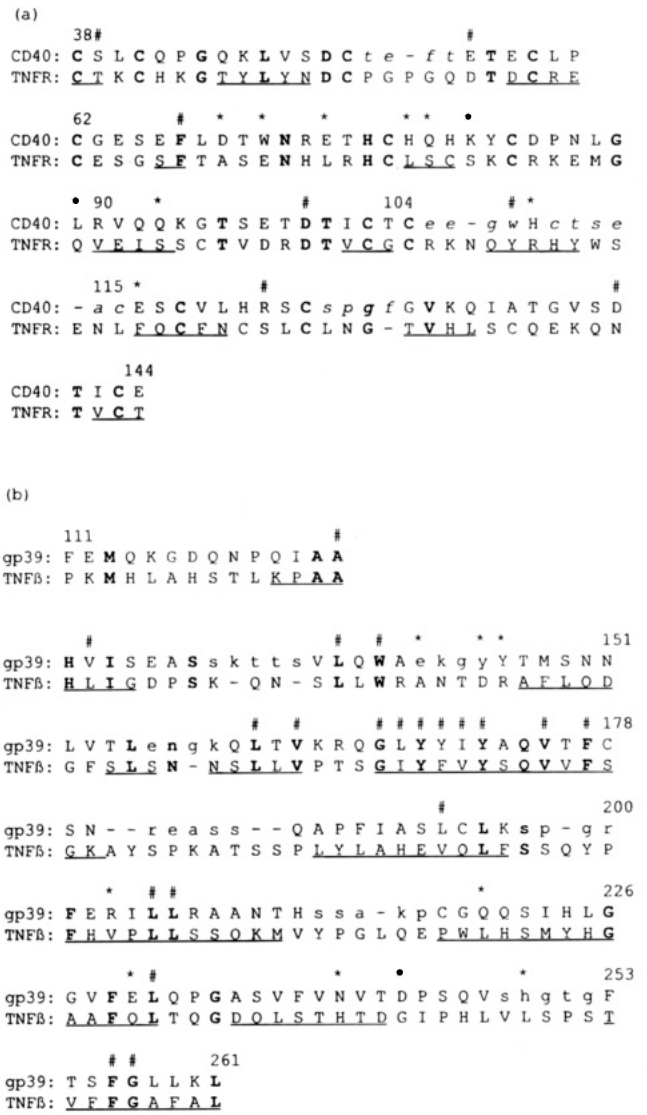

FIGURE 1: CD40 vs TNFR and gp39 vs TNF-β sequence alignments. The structure-oriented sequence alignments provided the basis for modeling CD40 and gp39, respectively. Sequence homologies for the regions included in (a) the CD40/TNFR and (b) the gp39/TNF-β alignments are 25−26%. Residue identities are shown in bold, and residues in CD40 and gp39 whose conformations were modeled using conformational search are given in lower case. Residues which were subjected to mutagenesis are labeled (*). Residue 62 in CD40 is the first residue of domain 2, residue 104 is the first residue of domain 3. In (a), (#) indicates residues thought to be critical (in addition to disulfide bonds) for the TNFR fold (Banner et al., 1993). Residues in β-strand segments are underlined. In (b), (#) denotes residues most conserved across the TNF family (Smith et al., 1994), and β-strands conserved in TNF-α and -β are underlined. Neither TNF nor TNFR contain α-helical elements.

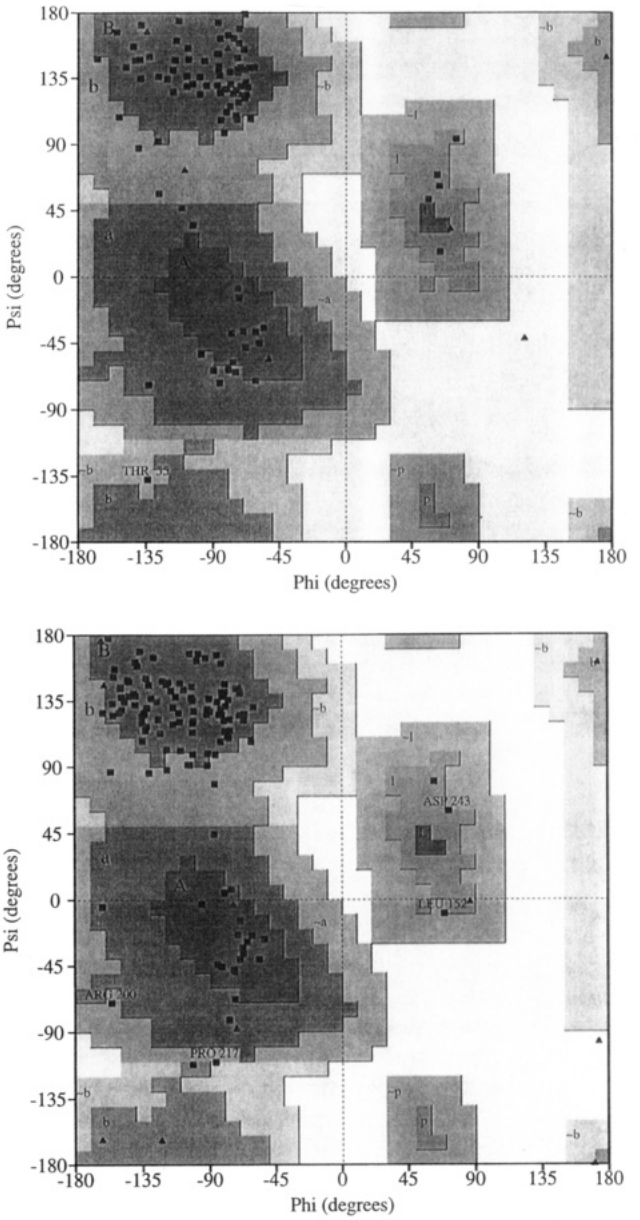

FIGURE 2: Analysis of ϕ/ψ main-chain torsion angles in the CD40 and gp39 models. Ramachandran diagrams (Ramachandran & Sasiekharan, 1968) for (a, top) the CD40 and (b, bottom) the gp39 models. Non-glycine residues are shown as squares and glycine residues as triangles. Regions populated by energetically favored main-chain torsion angles are shaded. Torsion angles in the nonshaded region are usually only found for glycines. All non-glycine residues in the models adopt energetically allowed ϕ/ψ angles. The figure was generated with PROCHECK (Laskowski et al., 1993).

of gp39 and CD40 was based. These alignments are an extension of our previous alignment (Bajorath et al., 1995) and include secondary structure information, key structural residues, all modeled regions, and conformational search derived segments. The gp39 monomer model includes residues 111−261, and the CD40 model includes residues 38−144. Prior to the availability of the TNF-β/TNFR coordinates, our first gp39 model (Aruffo et al., 1993) was based on the TNF-α structure (Eck & Sprang, 1989). The backbone rms deviation, including all residues, between these two gp39 monomer models is ~1.4 Å, reflecting differences in backbone regions of the structural templates and in loop regions of the models. The initially assembled gp39 and CD40 models were energy minimized until the rms derivative of the energy function was less than 1 kcal/Å. At this stage, the core regions of both models displayed backbone rms deviations of ~0.6 Å from their respective parent structures. When assessed with PROCHECK, both models displayed good stereochemistry and no unfavorable intramolecular contacts. Figure 2 shows that all non-glycine residues in both models adopt favorable main-chain torsion angles. Position-dependent energy profiles (Sippl, 1993) were calculated for both models and compared to the profiles of their crystallographic templates. This analysis is shown in Figure 3. In both cases, the overall similarity in shape and average energy of the profiles suggests sequence−structure compat-

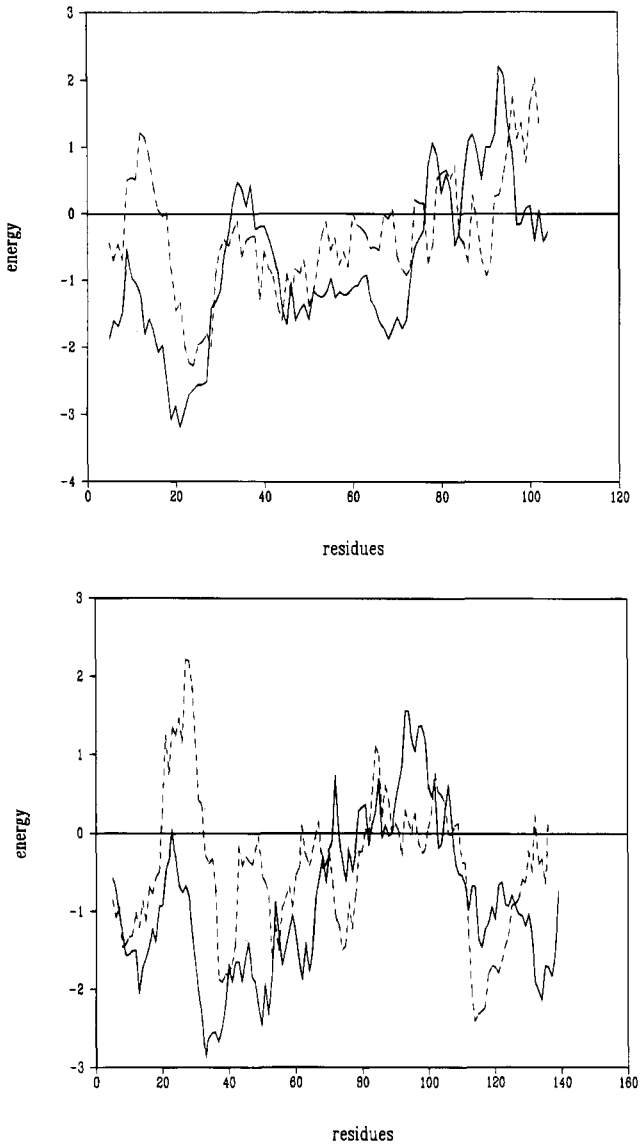

FIGURE 3: Energy profile analysis of the gp39 and CD40 models. Position-dependent energy profiles are calculated and overlayed for (a, top) the CD40 model (dashed line) and the TNFR X-ray structure (solid line) and (b, bottom) the gp39 monomer model (dashed line) and the TNF-β X-ray structure (solid line). Pairwise residue interaction energy is given as E/kt (E, interaction energy in kcal/mol; k, Boltzmann constant; T, absolute temperature in K). At each position, interaction energy values were averaged over 10 residues. The figure was generated with PROSAII (Sippl, 1993).

ibility of the models and the correctness of their global folds (Sippl, 1993).

Starting from the gp39 monomer, a trimeric form was generated by applying 3-fold symmetry operations (Banner et al., 1993). Since residues which mediate trimerization in TNF are conserved or conservatively replaced in gp39, the symmetrical interface of the gp39 trimer did not require further contact optimization. Figure 4a shows a representation of the trimeric form of the TNF-β-based gp39 model. The extracellular region of CD40 and other members of the TNFR family include four homologous domains. The molecular model of CD40 includes domains 2 and 3 and a fragment of domain 1. Parts of domain 1 and the entire domain 4 could not be modeled since the corresponding regions in TNFR were tentative or not visible in the X-ray structure. The CD40 model suggests the presence of a number of complementary ionic interactions thought to stabilize the structure. Figure 4b shows the modeled CD40 fragment. Two disulfide bonds in each of the TNFR domains are conserved in CD40. In domains 2 and 3, these are Cys62−Cys77 and Cys83−Cys103 (domain 2) and Cys105−Cys119 and Cys125−Cys143 (domain 3). The model suggests that CD40 contains an additional disulfide bond (Cys111−Cys116) which is not conserved in TNFR. Likewise, the gp39 monomer is predicted to contain a disulfide bond (Cys178−Cys218) which is not present in TNF-α or -β. Panels a and b of Figure 4 show the predicted disulfide bonds in gp39 and CD40, respectively. The presence of additional disulfide bonds in both models (rather than free cysteines) supports the validity of the sequence−structure alignments on which the modeling was based.

Molecular Model of the gp39−CD40 Complex. We have attempted to generate models of CD40 in complex with gp39 to approximate their interaction. Due to the limitations of model building, generation of such complexes is difficult, and details can often not be predicted with certainty. Thus, we have taken the conservative approach of superposing backbone segments thought to be conserved in gp39 and TNF-β and in CD40 and TNFR, respectively, based on the hypothesis that the gross interactions between the homologous TNF-β/TNFR and gp39/CD40 ligand/receptor pairs should be similar. The TNF-β/TNFR complex shows three equivalent symmetry-related binding sites, and each TNF-β/TNFR interface involves molecular contacts between two adjacent TNF-β monomers and one receptor molecule (Banner et al., 1993). TNF-β subunits A and C and the bound TNFR monomer were selected as targets for superposition of the models. The gp39 model was superposed on subunit A and on subunit C of TNF-β using the backbone atoms of superposition set S1 (gp39: 124, 126, 138, 140, 161, 163, 167, 168, 169, 170, 171, 172, 175, 177, 193, 205, 206, 231, 256, 257) and the corresponding residues in TNF-β (Figure 1). The backbone rms deviation for both superpositions was ~0.4 Å. The CD40 model was superposed on the TNFR monomer using the backbone atoms of superposition set S2 (CD40: 38, 51, 57, 59, 62, 67, 77, 83, 100, 101, 103, 119, 125, 141) and the corresponding residues in TNFR (Figure 1). The rms deviation for this superposition was ~0.6 Å. In the initial complex, only a few short gp39/CD40 contacts were observed. It was possible to correct these short contacts by manual side-chain adjustment. Contacts at the interface were refined by some minor energy minimization. Figure 4c shows the gp39/CD40 model complex obtained by superposition. Using computer graphics analysis, gp39 and CD40 residues were determined which were in van der Waals contact distance or close to contact distance. These included five loops (from peripheral to central positions at the interface: CD40, 112−115; gp39 monomer C, 197−200; CD40, 63−66; gp39 monomer A, 142−145, 248−252) and additional residues (gp39 monomer A, 124, 130, 131, 133, 146, 178, 216, 220, 245, 246; gp39 monomer C, 166, 186, 201, 202, 203, 204, 207, 229, 230, 232, 242; CD40, 69, 70, 71, 73, 74, 75, 76, 78, 79, 81, 82, 85, 84, 86, 87, 117, 118).

The initial gp39/CD40 interface obtained by superposition (called here version 1) was systematically remodeled by conformational search of only the side chains of all residues at the interface (as listed above) (version 2) or only the five loop conformations (modeled in the order given above) (version 3) or all side-chain and loop conformations (version

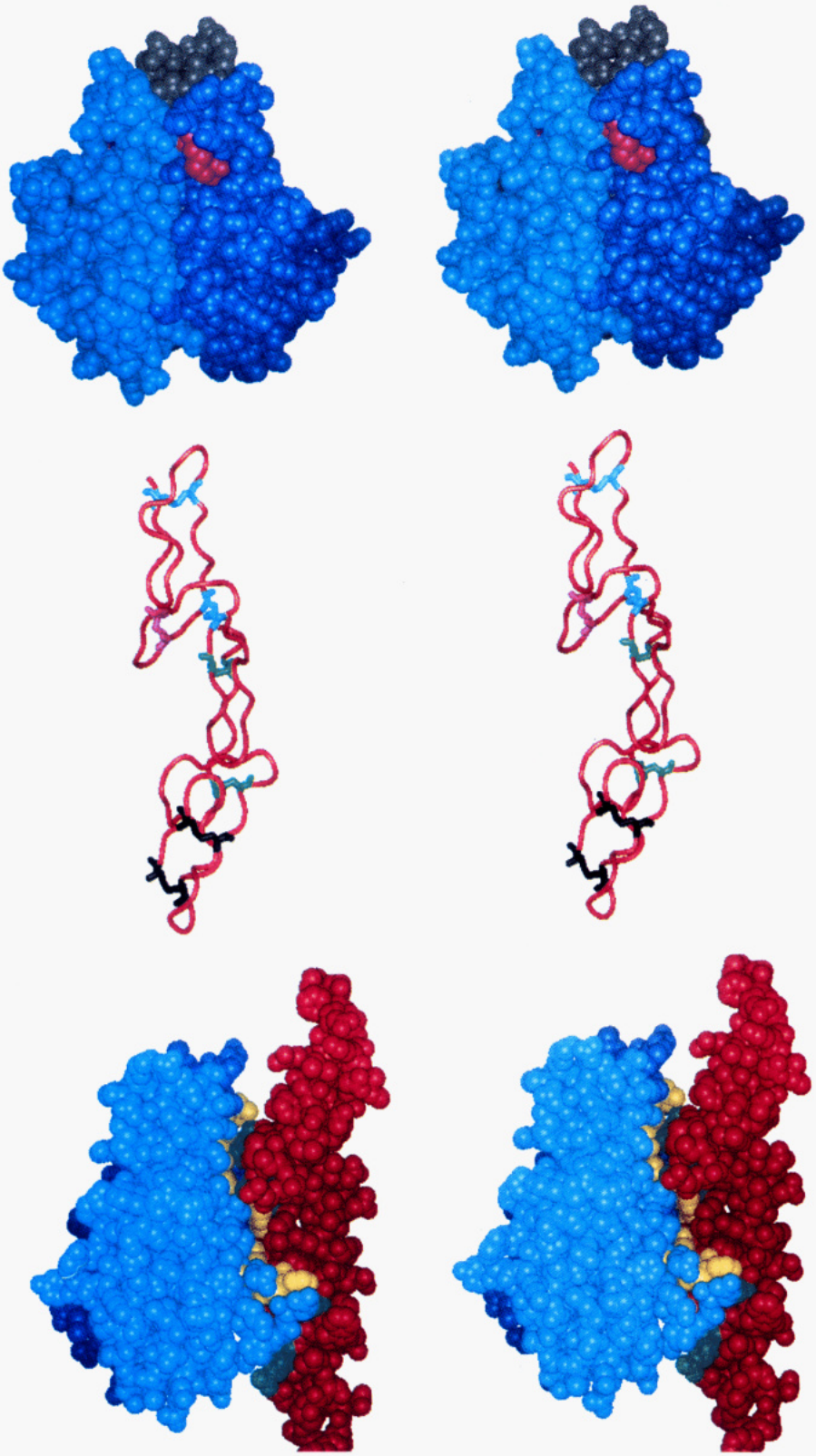

FIGURE 4: Molecular models of gp39, CD40, and their approximate interaction. Stereoviews are shown of (a, top) the TNF-β-based gp39 model, (b, middle) the CD40 model, and (c, bottom) the approximate gp39/CD40 interface, obtained by superposition of the models on their crystallographic counterparts (version 1, see text). (a) Space-filling representation of the trimeric form of the gp39 model, obtained from the monomer by applying 3-fold symmetry operations. Monomer A (front right) is colored dark blue, monomer B (back) is colored gray, and monomer C (front left) is colored light blue. The cysteines which form the predicted disulfide bond in gp39 are colored magenta and can be seen in the A monomer. (b) Solid ribbon representation of the CD40 model (red) highlighting the predicted disulfide bonds. Disulfide bonds which are conserved in CD40 and TNFR are shown in black (domain 1), green (domain 2), and blue (domain 3). The predicted domain 3 disulfide bond unique to CD40 (Cys 111−Cys116) is colored magenta. (c) Space-filling representation of the putative gp39/CD40 interface. One of the three equivalent binding sites in the complex is modeled, consisting of gp39 monomers A and C and CD40. Relative to (a) and (b), the orientation is obtained by ~90° rotation around the vertical axis. Residues in gp39 (monomer A, dark blue; monomer C, light blue) and CD40 (red) which were consistently buried in all modeled versions of the complex (as determined by solvent-accessible surface calculations, see text) are colored in yellow and green, respectively.

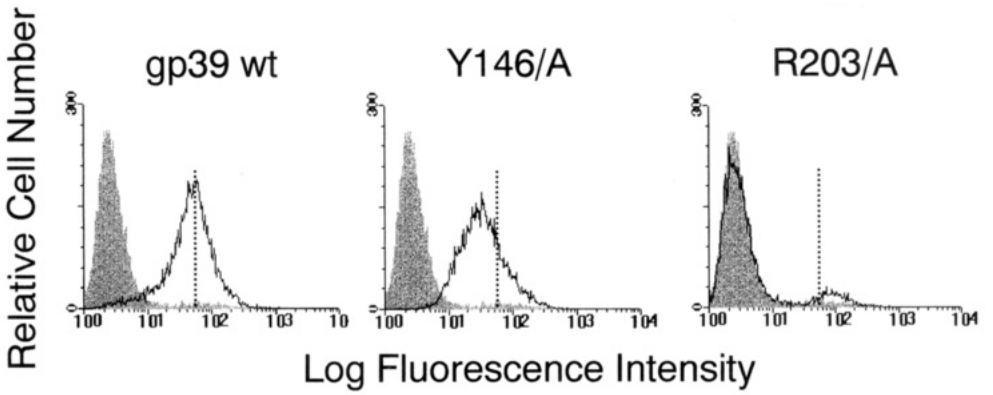

FIGURE 5: FACS profiles of representative cell binding experiments: Binding of wild-type and selected mutant $_s$gp39 to cells expressing CD40. Representative flow cytometry profiles of wild-type and mutant $_s$gp39 binding to Raji cells are shown. As a control, cells were stained with supernatants from mock-transfected COS cells (filled profiles in each histogram). The mutant label is shown above each profile. The dotted bar denotes the location of the peak channel for the binding of wild-type $_s$gp39 to Raji cells. Binding assays were carried out with saturating amounts of $_s$gp39 wild-type and mutant proteins. These FACS profiles are representative of the cell binding experiments with gp39 mutants and CD40 mutants which are summarized in Table 1. The FACS profile of gp39 mutant Y146/A represents significantly reduced cell binding ("+/−" in Table 1), and mutant R203/A represents no detectable cell binding ("−" in Table 1) relative to wild-type binding ("+" in Table 1).

4). We have calculated the contact surface in each version of the complex, defined here as the mean of the solvent-accessible surface area buried between the two gp39 monomers and CD40. The calculated contact surfaces were 1123 Å^2 (version 1), 939 Å^2 (version 2), 1066 Å^2 (version 3), and 931 Å^2 (version 4). These contact surface areas are comparable in size to the contact surface calculated for the TNF-β/TNFR X-ray structure (1130 Å^2) (Banner et al., 1993). Residues involved in interface interactions in versions 1−4 of the complex were determined by calculating differences in solvent-accessible surfaces (probe radius 1.4 Å) of gp39 and CD40 in the complex and in isolated form. The residues in gp39 and CD40 which buried consistently at least 20 Å^2 of solvent-accessible surface area in the putative complexes were, in gp39 monomer A, A130, S131, K143, E144, Y145, Y146, C178, N180, C218, Q220, S248, and H249, in gp39 monomer C, F201 and R203, and, in CD40, S65, T70, R73, E74, H76, H78, Y82, D84, P85, N86, and A115. Thus, these residues may be involved in the formation of the gp39/CD40 interface.

Selection of Residues for Mutagenesis. Residues consistently involved in the formation of the modeled gp39/CD40 interface were examined as to their suitability for mutagenesis. Some residues were not selected because main-chain atoms contributed largely to burial of solvent-accessible surface area, while others (Pro, Cys) were not selected as their replacement may lead to structural perturbations. Following these considerations, we selected two CD40 residues (E74 and H78) and four gp39 residues (Y146, R203, Q220, and H249) for mutagenesis. In addition, we selected four gp39 (E142, E230, N240, D243) and four CD40 residues (D69, W71, Q79, E117) which were involved in, or proximal to, the modeled interface and whose positions corresponded to ligand−receptor contact residues in the TNF-β/TNFR complex (Banner et al., 1993). As controls, we selected four additional CD40 residues (K81, L89, Q93, H110) whose positions did not correspond to contact residues in the TNF-β/TNFR complex. Previously, we showed that the gp39 mutant Y145/A and CD40 mutant Y82/A failed to bind CD40 and gp39, respectively (Bajorath et al., 1995). To further assess the contribution of these residues to the gp39/CD40 interaction, we replaced these residues with Phe. Taken together, nine mutagenesis experiments on gp39 and eleven mutagenesis experiments on CD40 were carried out.

Preparation of gp39 and CD40 Mutants. All selected residues were mutated to Ala (or Phe) in the soluble fusion proteins of gp39 and CD40. The amount of each of the $_s$gp39 (soluble recombinant form of gp39) and CD40-Ig (soluble recombinant form of CD40) mutants transiently produced by COS cells was examined by SDS−PAGE (data not shown). This analysis showed that one of the nine gp39 (N240/A) and two of the eleven CD40 (W71/A and H78/A) mutant proteins were not expressed in sufficient quantities to allow further studies.

Characterization of gp39 and CD40 Mutants. The structural integrity of the remaining gp39 and CD40 mutants was indirectly assessed by examining their ability to bind to panels of five different anti-gp39 or anti-CD40 mAbs which recognize distinct epitopes (Bajorath et al., 1995). gp39 mutants E230/A and H249/A did not bind to any of the mAbs, and mutant D243/A bound only at very low levels. The other gp39 mutants bound strongly to all anti-gp39 mAbs. All CD40 mutants bound to at least four of the five anti-CD40 mAbs (mAb 40-1.62 did not bind to the mutant L89/A; mAb 40-1.87 failed to bind to CD40 mutants Q93/A, D69/A, and K81/A). In our previous study we found that CD40 mutant Y82/A failed to bind to the anti-CD40 mAb 40-2.131. However, replacing Y82 with Phe resulted in a CD40 mutant which was now able to bind mAb 40-2.131 as well as to the other mAbs tested. Although we cannot rule out the possibility that some of the mutations simultaneously affect different epitopes recognized by the mAbs in our panel, we performed binding studies only with mutants that consistently bound to at least four mAbs in each panel. Thus, five gp39 and nine CD40 mutants were subjected to binding studies.

Binding of gp39 Mutant Proteins to CD40. We examined the ability of the mutant gp39 proteins to bind CD40 in two different assays. In the first assay, the binding of wild-type and mutant $_s$gp39 to CD40 expressed on the surface of the B cell line Raji was examined by flow cytometry. Figure 5 shows the results of representative cell binding experiments. The data are summarized in Table 1. In this assay, gp39 mutant R203/A did not bind to the Raji cells, while mutants

Table 1: Binding of gp39 and CD40 Mutant Proteins[a]

CD40 mutant binding (%)			gp39 mutant binding (%)		
	ELISA	FACS		ELISA	FACS
CD40 wt	100 ± 3	+	gp39 wt	100 ± 21	+
Leu8	14 ± 1	−	mock	9 ± 2	−
D69/A	79 ± 4	+	E142/A	92 ± 8	+
E74/A	8 ± 2	−	Y145/F	82 ± 4	+
Q79/A	66 ± 3	+	Y146/A	18 ± 7	+/−
K81/A	104 ± 3	+	R203/A	9 ± 6	−
Y82/F	16 ± 2	−	Q220/A	58 ± 7	+
L89/A	98 ± 13	+			
Q93/A	105 ± 5	+			
H110/A	72 ± 3	+			
E117/A	50 ± 2	+/−			

[a] The binding of CD40 and gp39 mutants to $_s$gp39 and CD40-Ig, respectively, by ELISA is reported as percent of wild-type binding. The binding of CD40 and gp39 mutants to BMS-10 and Raji cells, respectively, by FACS analysis is reported relative to wild type as + (binding comparable to wild type or slightly reduced), +/− (binding significantly reduced), or − (no detectable binding). See Figure 5 for representative FACS profiles and Figures 6 and 7 for representative ELISA curves.

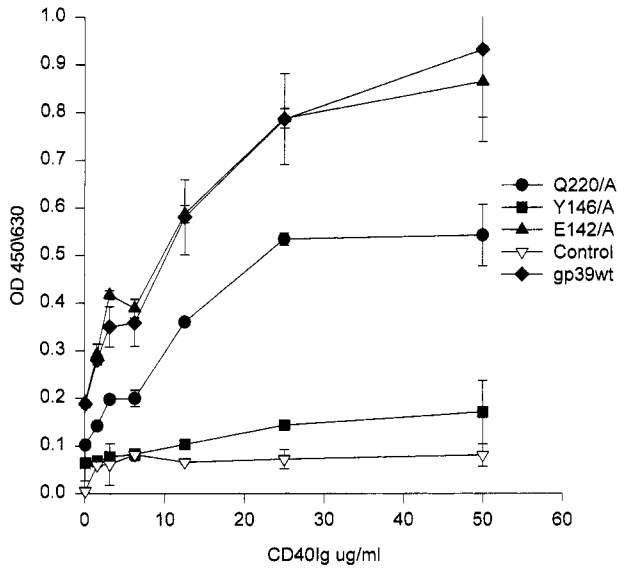

FIGURE 6: Binding of immobilized wild-type and mutant $_s$gp39 to CD40-Ig. Wild-type and mutant $_s$gp39 were immobilized on plastic as described in the Materials and Methods section. The binding of increasing concentrations of CD40-Ig to the immobilized $_s$gp39 proteins was monitored by ELISA. Error bars represent standard deviations of triplicate analysis. Supernatants of mock transfected cells were used as negative control.

Y146/A showed significantly reduced and Q220/A slightly reduced binding when compared to gp39 wild type. gp39 mutants Y145/F and E142/A bound to Raji cells comparably to wild type. In the second binding assay, the ability of wild-type or mutant gp39 immobilized on plastic to bind to CD40-Ig was examined (Figure 6 and Table 1). The results parallel those obtained by FACS analysis. In this assay, gp39 mutants Y146/A and R203/A showed significantly reduced and Q220/A partially reduced CD40-Ig binding, while mutants Y145/F and E142/A bound like wild type. These results show that gp39 residues Y146, Q220, and R203 participate in gp39 interactions and that the size (Tyr/Phe vs Ala) of gp39 residue 145 is critical for gp39/CD40 binding.

Binding of CD40 Mutant Proteins to gp39. The ability of wild-type and mutant CD40 to bind to gp39 was also

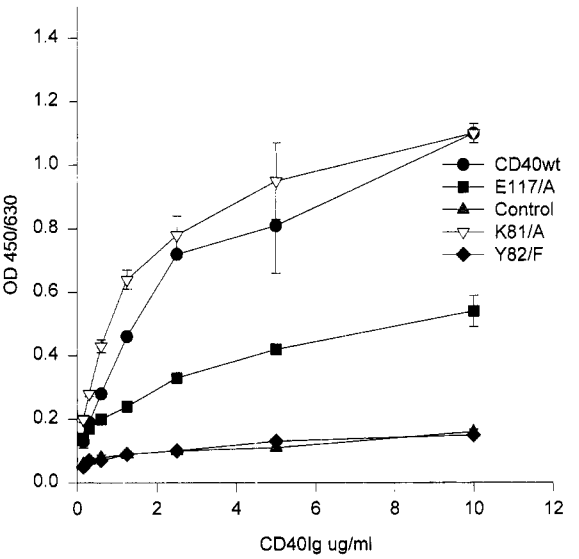

FIGURE 7: Binding of immobilized $_s$gp39 to wild-type and mutant CD40-Ig. The binding of increasing concentrations of wild-type and mutant CD40-Ig to $_s$gp39 immobilized on plastic was monitored by ELISA. The $_s$gp39 was immobilized on plastic as described in the Materials and Methods section. Error bars represent standard deviations of triplicate analysis. Binding of Leu8-Ig was used as a negative control.

examined in two assays. In the first assay the binding of wild-type and mutant CD40-Ig to the T cell line BMS-10, which constitutively expresses gp39, was examined by flow cytometry (Table 1). In this assay, CD40 mutants E74/A and Y82/F showed no binding to BMS-10 cells while mutant E117/A showed significantly reduced binding. Mutants D69/A, Q79/A, K81/A, Q93/A, H110/A, and L89/A bound BMS-10 cells at levels similar to wild-type CD40-Ig. In the second assay, the ability of wild-type and mutant CD40-Ig to bind to $_s$gp39 immobilized on plastic was measured by ELISA. The data from these experiments parallel what was found in the cell binding assays (Table 1). Representative binding curves for the ELISA assay are shown in Figure 7. These results show that three CD40 mutants (E74/A, Y82/F, and E117/A) had significantly reduced binding to gp39. Although the conservative CD40 mutant Y82/F bound all mAbs tested, including mAb 40-2.131, it failed to bind wild-type gp39 in both assay systems. Thus, the absence of the hydroxy group on CD40 residue Y82 is sufficient to severely compromise the gp39/CD40 interaction.

Summary of Mutagenesis Studies. In this study, we have identified three gp39 residues (Y146, R203, and Q220) and two CD40 residues (E74 and E117) as important for the gp39/CD40 interaction. Despite their limitations and inherent approximations, the gp39/CD40 models aided substantially in the identification of these residues. Four of these five residues (all except E117) belonged to the set of residues which consistently buried at least 20 Å^2 of solvent-accessible surface in all versions of the modeled gp39/CD40 complex and which were, therefore, selected for mutagenesis. That these residues indeed participate in critical gp39/CD40 interactions supports the existence of structural similarity of the gp39/CD40 and TNF-β/TNFR ligand/receptor complexes and, in addition, demonstrates the usefulness of the modeling study for targeted mutagenesis on gp39 and CD40.

In our previous mutagenesis study (Bajorath et al., 1995), residues were selected for replacement on the basis of

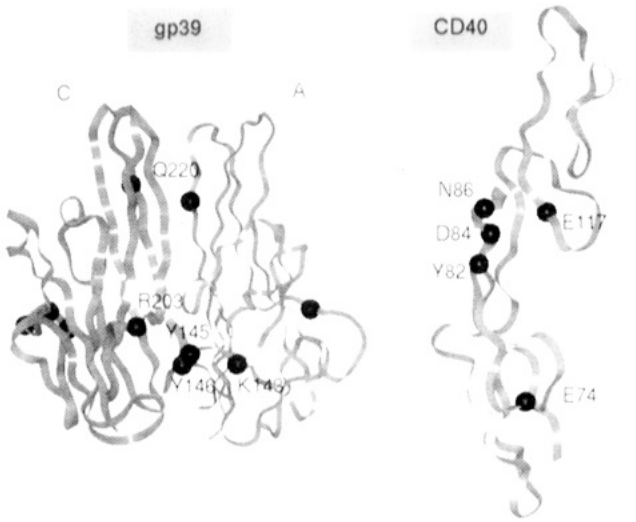

FIGURE 8: Residues important for the gp39 and CD40 interaction. The location of gp39 and CD40 residues which, when mutated, compromise the gp39/CD40 interaction are mapped on ribbon representations of the CD40 and gp39 [monomers A (small ribbon) and C] molecular models. The α-carbon positions of these residues are depicted as black spheres. The view is facing the putative contact areas.

sequence alignments and the crystallographic contact map of TNF-β/TNFR (Banner et al., 1993). In summary, these two studies have resulted in the identification of five gp39 residues (K143, Y145, Y146, R203, Q220) and five CD40 residues (E74, Y82, D84, N86, E117) that substantially contribute to the gp39/CD40 interaction. A contribution of N-linked glycosylation to the gp39/CD40 interaction is unlikely since the studied CD40 fragment contains no N-linked glycosylation sites and since mutation of N240, the only N-linked glycosylation site in the TNF-homologous region of gp39, does not affect gp39/CD40 binding (Bajorath et al., 1995).

Outline of gp39 and CD40 Binding Sites. Figure 8 shows the predicted location of the critical gp39 and CD40 residues when mapped on our gp39 and CD40 models, respectively. Two loop regions, K143−Y146 in gp39 and Y82−N86 in CD40, have been identified as "hot spots" for the gp39/CD40 interactions. In addition, four of five critical residues in gp39 (except Q220) and CD40 (except E74) cluster on gp39 and CD40, respectively. Analysis of the location in the model of residues which are critical for the gp39/CD40 interaction suggests that residue Q220 in gp39 interacts with residues in or proximal to the cluster of CD40 residues involved in gp39 binding and that residue E74 in CD40 interacts with residues in or proximal to the cluster of gp39 residues involved in CD40 binding. Our results suggest the presence of at least two regions in gp39 and CD40 which determine their interaction. gp39 residue R203 participates in the gp39/CD40 interaction, and this suggests that residues of two adjacent gp39 monomers are involved in the formation of the CD40 binding site (Figure 8). The regions outlined as the gp39/CD40 binding site essentially correspond to regions in TNF-β/TNFR which include critical contact residues (Banner et al., 1993; Van Ostade et al., 1994). However, these residues are not conserved in gp39/CD40.

Conclusion. Using a combination of molecular modeling, site-directed mutagenesis, monoclonal antibody binding, and receptor−ligand binding assays presented herein and in our previous study (Bajorath et al., 1995), we have identified ten residues, five in gp39 and five in CD40, which substantially contribute to the gp39/CD40 interaction. The predicted location of these gp39 and CD40 residues is consistent with the presence of gp39/CD40 contacts that are formed along the interface of two gp39 monomers and involve distinct clusters of residues. In this regard, these results parallel those obtained for the TNF-β/TNFR system. Residues implicated in gp39/CD40 interactions are not conserved in TNF-β/TNFR and *vice versa*, which is consistent with the specificity of the respective interactions.

ACKNOWLEDGMENT

We thank Dr. R. Mittler for providing the BMS-10 cell line, Dr. J. Ledbetter for providing mAbs G28-5 and 53.6, and Debby Baxter for help in preparing the manuscript.

REFERENCES

Alderson, M. R., Armitage, R. J., Tough, T. W., Strockbine, L., Fanslow, W. C., & Spriggs, M. K. (1993) *J. Exp. Med. 178*, 669.

Allen, R. C., Armitage, R. J., Conley, M. E., Rosenblatt, H., Jenkins, N. A., Copeland, N. G., Bedell, M. A., Edelhoff, S., Disteche, C. M., Simoneaux, D. K., Fanslow, W. C., Belmont, J., & Spriggs, M. K. (1993) *Science 259*, 990.

Armitage, R. J., Fanslow, W. C., Strockbine, L., Sato, T. A., Clifford, K. N., Macduff, B. M., Anderson, D. M., Gimpel, S. D., Davis-Smith, T., Maliszewski, C. R., Clark, E. A., Smith, C. A., Grabstein, K. H., Cosman, D., & Spriggs, M. K. (1992) *Nature 357*, 80.

Aruffo, A., Farrington, M., Hollenbaugh, D., Li, X., Milatovich, A., Nonoyama, S., Bajorath, J., Grosmaire, L. S., Stenkamp, R., Neubauer, M., Roberts, R. L., Noelle, R. J., Ledbetter, J. A., Francke, U., & Ochs, H. D. (1993) *Cell 72*, 291.

Bajorath, J., & Fine, R. M. (1992) *Immunomethods 1*, 137.

Bajorath, J., Stenkamp, R., & Aruffo, A. (1993) *Protein Sci. 2*, 1798.

Bajorath, J., Chalupny, N. J., Marken, J. S., Siadak, A. W., Skonier, J., Gordon, M., Hollenbaugh, D., Noelle, R. J., Ochs, H. D., & Aruffo, A. (1995) *Biochemistry 34*, 1833.

Banner, D. W., D'Arcy, A., Janes, W., Gentz, R., Schoenfeld, H.-J., Broger, C., Loetscher, H., & Lesslauer, W. (1993) *Cell 73*, 431.

Beutler, B., & van Huffel, C. (1994) *Science 264*, 667.

Bruccoleri, R. E., & Novotny, J. (1992) *Immunomethods 1*, 96.

Clark, E. A., & Ledbetter, J. A. (1986) *Proc. Natl. Acad. Sci. U.S.A. 83*, 4494.

Di Santo, J. P., Bonnefoy, J. Y., Gauchat, J. F., Fischer, A., & de Saint-Basile, G. (1993) *Nature 361*, 541.

Durandy, A., Schiff, C., Bonnefoy, J. Y., Forveille, M., Rousset, F., Mazzei, G., Milili, M., & Fischer, A. (1993) *Eur. J. Immunol. 23*, 2294.

Durie, F. H., Fava, R. A., Foy, T. M., Aruffo, A., Ledbetter, J. A., & Noelle, R. J. (1993) *Science 261*, 1328.

Eck, M. J., & Sprang, S. R. (1989) *J. Biol. Chem. 264*, 17595.

Eck, M. J., Ultsch, M., Rinderknecht, E., de Vos, A. M., & Sprang, S. R. (1992) *J. Biol. Chem. 267*, 2119.

Farrah, T., & Smith, C. A. (1992) *Nature 358*, 26.

Foy, T. M., Shepherd, D. M., Durie, F. H., Aruffo, A., Ledbetter, J. A., & Noelle, R. J. (1993) *J. Exp. Med. 178*, 1567.

Fuleihan, R., Ramesh, N., Loh, R., Jabara, H., Rosen, R. S., Chatila, T., Fu, S. M., Stamenkovic, I., & Geha, R. S. (1993) *Proc. Natl. Acad. Sci. U.S.A. 90*, 2170.

Graf, D., Korthauer, U., Mages, H. W., Senger, G., & Kroczek, R. A. (1992) *Eur. J. Immunol. 22*, 3191.

Hermann, P., Blanchard, D., de Saint-Vis, B., Fossiez, F., Gaillard, C., Vanbervliet, B., Briere, F., Banchereau, J., & Galizzi, J.-P. (1993) *Eur. J. Immunol. 23*, 961.

Ho, S. N., Hunt, H. D., Horton, R. M., Pullen, J. K., & Pease, L. R. (1989) *Gene 77*, 51.

Hollenbaugh, D., Grosmaire, L. S., Kullas, C. D., Chalupny, N. J., Braesch-Andersen, S., Noelle, R. J., Stamenkovic, I., Ledbetter, J. A., & Aruffo, A. (1992) *EMBO J. 11*, 4313.

Jones, E. Y., Stuart, D. I., & Walker, N. P. C. (1989) *Nature 338*, 225.

Korthauer, U., Graf, D., Mages, H. W., Briere, F., Padayachee, M., Malcolm, S., Ugazio, A. G., Notarangelo, L. D., Levinsky, R. J., & Kroczek, R. A. (1993) *Nature 361*, 539.

Lane, P., Traunecker, A., Hubele, S., Inui, S., Lanzaveccia, A., & Gray, D. (1992) *Eur. J. Immunol. 22*, 2573.

Laskowski, R. A., MacArthur, M. W., Moss, D. S., & Thornton, J. M. (1993) *J. Appl. Crystallogr. 26*, 283.

Lederman, S., Yellin, M. J., Cleary, A. M., Pernis, A., Inghirami, G., Cohn, L. E., Covery, L. R., Lee, J. J., Rothman, P., & Chess, L. (1994) *J. Immunol. 152*, 2163.

Lee, B. K., & Richards, F. M. (1971) *J. Mol. Biol. 55*, 379.

Noelle, R. J., Roy, M., Shepherd, D. M., Stamenkovic, I., Ledbetter, J. A., & Aruffo, A. (1992) *Proc. Natl. Acad. Sci. U.S.A. 89*, 6550.

Paulie, S., Ehlin-Hendricksson, B., Mellstedt, H., Koho, H., Ben-Aissa, H., & Perlmann, P. (1985) *Cancer Immunol. Immunother. 20*, 23.

Ramachandran, G. N., & Sasiekharan, V. (1968) *Adv. Protein Chem. 23*, 283.

Sippl, M. (1993) *Proteins 17*, 355.

Smith, C. A., Farrah, T., & Goodwin, R. G. (1994) *Cell 76*, 959.

Spriggs, M. K., Armitage, R. J., Stockbine, L., Clifford, K. N., Macduff, B. M., Sato, T. A., Maliszewski, C. R., & Fanslow, W. C. (1992) *J. Exp. Med. 176*, 1543.

Stamenkovic, I., Clark, E. A., & Seed, B. (1988) *EMBO J. 7*, 1053.

Van Ostade, X., Tavernier, J., & Fiers, W. (1994) *Protein Eng. 7*, 5.

Walz, G., Aruffo, A., Kolanus, W., Bevilacqua, M., & Seed, B. (1990) *Science 250*, 1132.

BI9504825